Monthly Notices
of the
ROYAL ASTRONOMICAL SOCIETY

MNRAS **456,** 4542–4550 (2016) doi:10.1093/mnras/stv2942

EU Del: exploring the onset of pulsation-driven winds in giant stars

I. McDonald,[1⋆] A. A. Zijlstra,[1] G. C. Sloan,[2] E. Lagadec,[3] C. I. Johnson,[4] S. Uttenthaler,[5] O. C. Jones[1,6] and C. L. Smith[1,7]

[1]*Jodrell Bank Centre for Astrophysics, Alan Turing Building, Manchester M13 9PL, UK*
[2]*Cornell Center for Astrophysics and Planetary Science, Cornell University, Ithaca, NY 14853-6801, USA*
[3]*Observatoire de la Côte d'Azur, Boulevard de l'Observatoire, CS 34229, F-06304 Nice Cedex 4, France*
[4]*Harvard–Smithsonian Center for Astrophysics, 60 Garden Street, MS–15, Cambridge, MA 02138, USA*
[5]*Department of Astrophysics, University of Vienna, Türkenschanzstraße 17, A-1180 Vienna, Austria*
[6]*STScI, 3700 San Martin Drive, Baltimore, MD 21218, USA*
[7]*Center for Research in Earth and Space Science (CRESS), York University, 4700 Keele Str, Toronto, ON M3J 1P3, Canada*

Accepted 2015 December 14. Received 2015 November 23; in original form 2015 September 21

ABSTRACT

We explore the wind-driving mechanism of giant stars through the nearby (117 pc), intermediate-luminosity ($L \approx 1600\ L_\odot$) star EU Del (HIP 101810, HD 196610). Atacama Pathfinder Experiment observations of the CO (3–2) and (2–1) transitions are used to derive a wind velocity of $9.51 \pm 0.02\ km\ s^{-1}$, a $^{12}C/^{13}C$ ratio of 14^{+9}_{-4} and a mass-loss rate of a few $\times\ 10^{-8}\ M_\odot\ yr^{-1}$. Analysis of published spectra show the star has a metallicity of [Fe/H] $= -0.27 \pm \sim 0.30$ dex. The star's dusty envelope lacks a clear 10-μm silicate feature, despite the star's oxygen-rich nature. Radiative transfer modelling cannot fit a wind acceleration model which relies solely on radiation pressure on condensing dust. We compare our results to VY Leo (HIP 53449), a star with similar temperature and luminosity, but different pulsation properties. We suggest the much stronger mass-loss from EU Del may be driven by long-period stellar pulsations, due to its potentially lower mass. We explore the implications for the mass-loss rate and wind velocities of other stars.

Key words: stars: AGB and post-AGB – circumstellar matter – stars: individual: EU Del – stars: mass-loss – stars: winds, outflows.

1 INTRODUCTION

The wind-driving mechanism of giant stars is poorly determined (e.g. Woitke 2006). Conventionally, low- and intermediate-mass stars (≈0.8–8 $M_\odot$) ascending the asymptotic giant branch (AGB) are thought to first exhibit a magneto-acoustically driven wind, which later transitions to a pulsation-enhanced, dust-driven wind (e.g. Dupree, Hartmann & Avrett 1984; Winters et al. 2000). Initially, magneto-acoustic waves propagating through the outer stellar atmosphere heat a stellar chromosphere providing energy for an outflow, either directly or via solar-like magnetic reconnection events. Later, κ-mechanism pulsations are stochastically excited by the star's large atmospheric convective cells. These pulsations levitate its outer atmosphere. The levitated material cools and condenses into dust. The opaque dust absorbs outgoing stellar radiation and re-radiates it isotropically, imparting net outward momentum, which forces it from the star. Collisional coupling with gas particles ejects the entire envelope into the interstellar medium (e.g. Habing 1996).

The mechanism by which the wind is ejected is important not only for modelling this stage of evolution, but also for its extrapolation outside well-measured environments. It is particularly important in metal-poor stars, hence the early Universe. Here, stars of a given mass are smaller and hotter, so a pulsation-driven wind must impart more energy to levitate material to the same dust-formation radius. Less refractory material means a lower dust-to-gas ratio, decreasing the efficacy and velocity of a dust-driven wind. Separation of gas and dust can occur, leading to a drift velocity, preventing the escape of the gas and perhaps depleting the star of dust-forming elements.

Despite this, prolific dust condensation is seen around metal-poor stars, indicating these stars somehow drive substantial stellar winds (Sloan et al. 2010; McDonald et al. 2011b). Dust production begins at ∼600–2000 $L_\odot$ (McDonald et al. 2011c; McDonald, Zijlstra & Boyer 2012; Momany et al. 2012). However, there is insufficient opacity to drive the wind, particularly among oxygen-rich stars, until the star reaches higher luminosities (Girardi et al. 2010). By measuring the wind expansion velocity and total mass-loss rate of stars as a function of properties such as luminosity and metallicity, we can determine the point at which the transition to a pulsation and/or dust-driven wind occurs.

Such measurements are usually derived from (sub-)mm CO lines. However, most metal-poor stars with well-known properties lie at

⋆E-mail: iain.mcdonald-2@manchester.ac.uk

Table 1. Properties of EU Del.

Parameter	Value	Ref.
RA	20 37 54.728	1
Dec	+18 16 06.89	1
Distance (d)	117 ± 7 pc	1
RA proper motion	+35.44 mas yr^{-1}	1
Dec proper motion	+61.57 mas yr^{-1}	1
Tangential velocity	38 km s^{-1}	
Radial velocity	–66 km s^{-1}	2
Spectral type	M6	3
Effective temperature ($T_{\rm eff}$)	3100 K	4
	3243 K	5
	3227 K	6
	3508 K	7
Luminosity (L)	1585 $L_\odot$	6
log(g)	0.39	4
Radius (R)	127.5 $R_\odot$	6
Assumed mass (M)	≈0.6 $M_\odot$	
Assumed initial mass	∼0.9 $M_\odot$	
Escape velocity for M	42 km s^{-1}	
Variability type	SRV (O-rich)	8
Period	59.7 d	9
	60.8, 132.6, 235.3, 67.3, 44.0 d	10
Amplitude (optical)	149, 113, 91, 75, 61 mmag	10
[Fe/H]	∼–1	4
	-0.27 ± 0.30	11
$^{12}C/^{13}C$	14^{+9}_{-4}	11

References: (1) van Leeuwen (2007); (2) de Bruijne & Eilers (2012); (3) Keenan & McNeil (1989); (4) Wu et al. (2011); (5) Cesetti et al. (2013); (6) McDonald et al. (2012); (7) Soubiran et al. (2010); (8) Mennessier et al. (2001); (9) Samus et al. (2006); (10) Tabur et al. (2009); (11) this work.

large distances, in globular clusters or dwarf galaxies. Their distance and interstellar radiation environment make them challenging to observe. A search for closer dust-producing giant stars with *Hipparcos* parallaxes identified several nearby targets (McDonald et al. 2012).

One of these targets was EU Del (HIP 101810, HD 196610), the stellar parameters of which are listed in Table 1. EU Del is among the closest bright giant stars. Table 1 lists its properties and Fig. 1 shows its spectral energy distribution (SED). It is a semiregular variable, with a characteristic period of ∼60 d (Samus et al. 2006). Wu et al. (2011) estimated that EU Del had a metallicity of [Fe/H] ∼ −1. However, their metallicity was poorly constrained and based on an automated fitting procedure that was not optimized for cool stars. An *IRAS* Low Resolution Spectrometer (LRS) spectrum of the star originally led it to be classified as 'naked' (i.e. not producing dust; Sloan & Price 1995). However, detailed modelling of the entire SED shows it to have considerable infrared excess, indicative of circumstellar dust (McDonald et al. 2012). Unusually for an oxygen-rich star, it does not show the typical 10-μm silicate or 11-μm alumina dust features, which partly explains the difference in classifications.[1] This is typical of metal-poor stars in globular clusters (McDonald et al. 2010). In this paper, we improve the determination of EU Del's metallicity and present new observations

[1] Sloan & Price (1995) detect a dust emission by determining a semi-empirical function to the stellar continuum between 7.67 and 14.03 μm. This is divided out and the normalized spectrum integrated. Stars with <8 per cent emission are classed as naked. Thus stars with a low-contrast infrared excess but no dust features in their spectra can still be classed as naked.

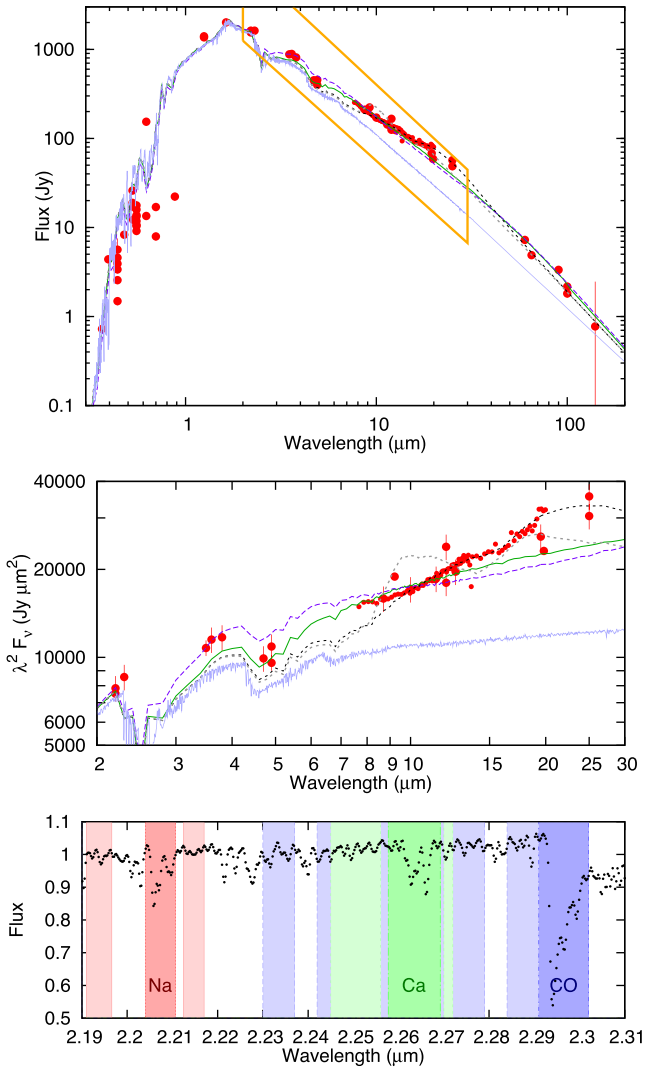

Figure 1. Top panel: SED of EU Del (large red points) including the *IRAS*-LRS spectrum (small red points), with a stellar atmosphere model (thin blue line) and DUSTY model fits (thicker green, purple, grey and black lines; see Section 3.1). The very thick orange parallelogram shows the portion expanded in the middle panel. See text for details of the models. Middle panel: the infrared portion of the spectrum, shown in Rayleigh–Jeans units to emphasize dust features. A naked stellar photosphere (thin blue line) should be roughly flat. A reddened spectrum indicates dust. Bottom panel: the *K*-band spectrum (Wallace et al. 2000) used for the metallicity determination, with line/continuum regions (dark/light boxes) marked for each line.

of the star's CO lines, placing its circumstellar wind in context with other mass-losing giant stars.

2 STELLAR PARAMETERS

2.1 Kinematic origin of EU Del

Anderson & Francis (2012) provide galactocentric velocity components for EU Del of $U = -64.3$, $V = -37.8$ and $W = +18.9$ km s^{-1}. They calculate that this velocity gives it an eccentric orbit, ranging in galactocentric radius from 4.5 to 8.4 kpc, implying that EU Del is close to apocentre. Using the Galactic Orbit Calculator,[2] we find

[2] http://www.astro.utu.fi/galorb.html

that the orbit of EU Del extends out of the plane by up to 300 pc. Thus, the star is normally around 150 pc from the plane.

Although the rotational velocity component (V) is large for a thin disc star (Ivezić, Beers & Jurić 2012), the extension from the plane is fairly small. The scaleheight of the thin disc and thick discs are ∼300 and ∼1350 pc, respectively, with the thick disc providing ∼2 per cent of the stars in the solar neighbourhood (Gilmore & Reid 1983). This translates to ∼3 per cent of stars at 150 pc from the plane, thus EU Del is most likely a thin disc star.

2.2 Metallicity of EU Del

2.2.1 Spectral discriminants

Strong molecular bands dominate the optical spectrum of EU Del (Valdes et al. 2004). These swamp the atomic lines normally used to determine stellar abundances. Near-IR spectra of EU Del (Wallace & Hinkle 1997; Meyer et al. 1998; Wallace et al. 2000, for the J, H and K_s bands, respectively) are not of sufficiently high resolution to enable detailed abundance measurements.

Instead, we compute [Fe/H] from the K-band spectrum (Wallace et al. 2000; Fig. 1), using the windowing functions of Ramírez et al. (2000) and Frogel et al. (2001). Ramírez et al. (2000) provide two methods to establish [Fe/H], based on the equivalent widths of the 2.21-μm Na doublet and 2.26-μm Ca triplet lines and the 2.29-μm CO $\nu = 2 \rightarrow 0$ bandhead. Both methods fit empirical second-order polynomials to spectra of 77 globular cluster giant stars, which have similar effective temperatures to our target. Method 1 is based only on the equivalent widths of the above spectral features. Method 2 also fits the $(J - K_s)$ colour and uses the M_{Ks} absolute magnitude of the star.

We use equations (3) and (4) of Frogel et al. (2001), which encode these two methods, to determine [Fe/H]. We measure equivalent widths of 3.53 ± 0.18, 2.63 ± 0.38 and 22.68 ± 0.53 Å for the Na, Ca and CO features, respectively. Methods 1 and 2 give [Fe/H] $= -0.30 \pm 0.05$ and -0.23 ± 0.06 dex, respectively.

The quoted errors are almost certainly underestimates, as no uncertainties are given on the fitting factors in either method. Based on the scatter of the [Fe/H] of individual stars from the 'known' cluster average (Frogel et al. 2001, their figs 11 and 12), we can expect the typical uncertainty to be ∼±0.2 dex.

We also note that no iron lines are used, thus the determination of [Fe/H] assumes a particular stellar composition. We must therefore account for the fact that the formalism is calibrated on α-enhanced stars in globular clusters. These stars are typically Ca-rich and C-poor, which have opposing effects on the abundance determination (Na abundance can vary; Roediger et al. 2014). Galactic field stars at [Fe/H] ≈ –0.3 dex have only slightly positive [Na/Fe] and [Ca/Fe] ratios (Edvardsson et al. 1993), which we estimate adds a further ∼±0.1 dex uncertainty on to the metallicity estimate. Taking these uncertainties and averaging between the two methods, we find [Fe/H] $= -0.27 \pm \sim 0.30$ dex.

2.2.2 Photometric discriminants

The position of EU Del in the Hertzsprung–Russell diagram (McDonald et al. 2012) is not significantly to the blue of the main red giant branch, as would be expected for a markedly metal-poor star (e.g. Marigo et al. 2008). However, interstellar reddening has not been taken into account. For giant stars, reddening of $E(B - V) = 0.01$ and $R_V = 3.1$ decreases the fitted effective temperature by ≈6 K (McDonald et al. 2009). The reddening towards EU Del is hard to compute as it is embedded within the Galaxy's thin disc. We have used the extinction maps of Lallement et al. (2014) to estimate that $E(B - V) \approx 0.015$, so it can be considered negligible.

EU Del is therefore most likely slightly metal-poor, but given the sizable and poorly quantified uncertainties on this measurement, we cannot reliably distinguish its metallicity from solar abundances. However, this value improves on existing determinations and contradicts the [Fe/H] $= -1$ value of Wu et al. (2011).

2.3 Wind velocity of EU Del

We obtained 230 GHz (850 μm) and 345 GHz (450 μm) observations of EU Del from the Swedish Heterodyne Facility Instrument (SHeFI) on the Atacama Pathfinder Experiment (APEX) telescope, on 2013 August 19 and 2014 August 18, respectively. We reduced the data using CLASS and XS.[3] Antenna temperature data were baseline subtracted by removing a straight line, fitted to the baseline flux. Temperatures were then converted to physical units using 39 Jy K^{-1} at 230 GHz and 41 Jy K^{-1} at 345 GHz[4]. Table 2 lists the resulting wind parameters.

These observations covered the ^{12}CO J=2–1, ^{12}CO J=3–2 and ^{13}CO J=3–2 transitions. Fig. 2 shows the spectra for these lines. The ^{12}CO lines shows rectangular profiles, consistent with an unresolved, optically thin line (the ^{13}CO line lacks the clarity needed to determine the shape accurately). A top-hat function was fit to each line using χ^2 minimization, with free parameters in expansion velocity (half-width), amplitude and central velocity. The best-fitting parameters were passed to the IDL optimization routine, MPFIT (Markwardt 2009), which uses the Levenberg–Marquardt technique to fit a least-squares, best-fitting model. MPFIT re-fitted the top-hat function (including a baseline offset) and computed the errors on the model parameters from the covariance matrix. From this, we derive the wind parameters listed in Table 2.

2.4 Mass-loss rate

An approximate mass-loss rate estimate can be obtained by using scaling relations derived from known stars. However, EU Del is relatively low luminosity and (perhaps) metal-poor compared to the stars for which these relations are calibrated. Such scaling relations are therefore poorly constrained in this regime. We adopt the relation of Ramstedt et al. (2008, their equation A.1) to produce the mass-loss rates in Table 2. To compute these, we have assumed beam sizes of 26.6 arcsec at 230 GHz and 17.3 arcsec at 345 GHz. We also assumed that Ramstedt's CO fraction (1/5000th of the wind at solar metallicity) decreases linearly with iron abundance. The formal errors are approximate, and the mass-loss rate can only be constrained to be between $\sim 10^{-8}$ and $\sim 10^{-7}$ M$_\odot$ yr^{-1}, thus we quote the mass-loss rate in the discussion as 'a few' $\times$ 10^{-8} M$_\odot$ yr^{-1}.

2.5 ^{12}C/^{13}C ratio

The ratio of the ^{12}CO (3–2) and ^{13}CO (3–2) lines provides a ^{12}C/^{13}C ratio for EU Del of 14^{+9}_{-4}, where the large uncertainty arising from the weak detection of the ^{13}CO line. This ratio is typical for a star which

[3] XS is a software package developed by P. Bergman to reduce and analyse single-dish spectra. It is publicly available from: ftp://yggdrasil.oso.chalmers.se.

[4] http://www.apex-telescope.org/telescope/efficiency/

Table 2. Wind parameters of EU Del from APEX observations

Parameter	Unit	^{12}CO J=2–1	^{12}CO J=3–2	^{13}CO J=3–2	Global
Frequency	GHz	230.538	345.796	330.587	–
Resolution	km s^{-1}	0.099	0.066	0.069	–
Noise	K	0.023	0.062	0.022	–
Intensity	K km s^{-1}	1.96 ± 0.04	3.57 ± 0.08	0.26 ± 0.12	–
Amplitude	K	0.1031 ± 0.0017	0.187 ± 0.004	0.013 ± 0.005	–
	Jy	4.02 ± 0.07	7.69 ± 0.16	0.54 ± 0.21	–
Half-width	km s^{-1}	9.492 ± 0.015	9.522 ± 0.019	9.86 ± 0.65	9.505 ± 0.021
Centre	km s^{-1}	-51.93 ± 0.04	-51.77 ± 0.04	-51.94 ± 0.60	-51.85 ± 0.10
Boxcar $\chi^2_{\rm red}$	–	1.087	1.322	1.224	–
$\dot{M}_{\rm Ramstedt}$	M$_\odot$ yr^{-1}	$5.1^{+7.5}_{-3.8} \times 10^{-8}$	$3.4^{+7.8}_{-3.2} \times 10^{-8}$	–	$4.7^{+5.3}_{-3.7} \times 10^{-8}$

Notes. Velocities are in the $v_{\rm LSR}$ frame, temperatures are antenna temperatures. The global mass-loss rate was produced by the logarithmic averaging of the ^{12}CO J=3–2 and 2–1 lines.

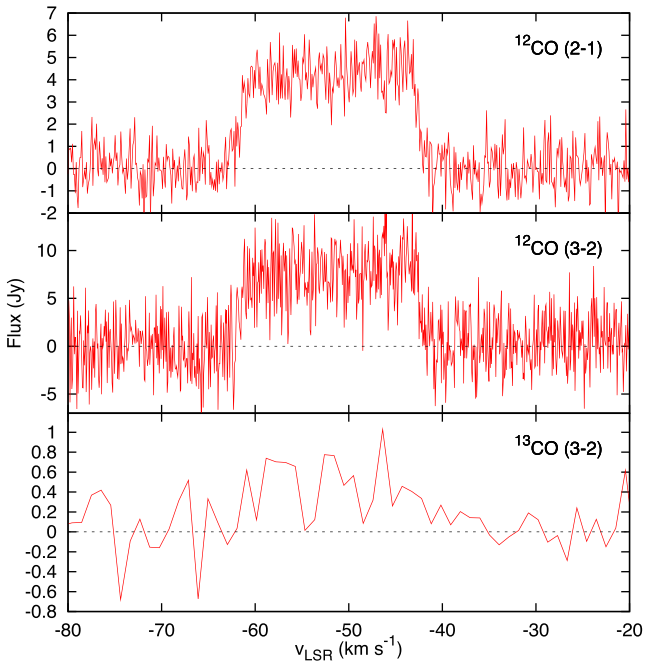

Figure 2. APEX spectra of EU Del. The ^{13}CO spectrum has been smooth to aid visibility.

has experienced first dredge-up but not third dredge-up (Karakas, private communication; see also, e.g. Reddy & Lambert 2005). It also matches the near-equilibrium values observed in metal-poor RGB-tip field stars (Gratton et al. 2000). However, the accuracy of this measurement depends on several assumptions.

(i) *The emission is optically thin.* This is attested by the flatness of the ^{12}CO line peaks, which will be more opaque than the ^{13}CO lines. An optically thick line would have produced a parabolic shape to the line.

(ii) *The ^{12}CO and ^{13}CO are emitted from the same region.* The optical thinness of the envelopes and similarity in the energy levels of ^{12}CO $J = 3$ and ^{13}CO $J = 3$ transitions (33.19 and 31.73 K, respectively) suggest the emission should come from very similar regions of the envelope.

(iii) *The ^{12}CO/^{13}CO ratio is equal to the ^{12}C/^{13}C ratio.* Selective photodissociation of ^{13}CO can occur if it is optically thin to UV radiation (>11.1 eV) and ^{12}CO is optically thick. Chemical fractionation can allow ^{13}CO to form preferentially, thus providing the opposite effect (e.g. Mamon, Glassgold & Huggins 1988; Vlemmings et al. 2013; Ramstedt & Olofsson 2014. This can provide an additional uncertainty of typically several tens of percent in the ^{12}C/^{13}C ratio. This uncertainty is not included here, as the wind of EU Del is optically thin in the ^{12}CO transitions.

3 THE WIND-DRIVING MECHANISMS

In this section, we explore the ability of three mechanisms to drive the wind: radiation pressure on dust, energy transfer from pulsations and release of magnetic energy from the stellar surface. In order to reproduce the minimum mass-loss rate and wind velocity listed in Table 2, a kinetically driven wind requires $\dot{E} = \dot{M}v^2/2 \gtrsim 2.7 \times 10^{22}$ W of kinetic energy, plus $\gtrsim 5.3 \times 10^{23}$ W of energy to overcome the gravitational potential ($\dot{E} = -GM\dot{M}/R$), or $\gtrsim 5.6 \times 10^{23}$ W in total.

3.1 A radiation-driven wind

In a radiation-driven wind, momentum from outgoing stellar photons is transferred to the dust grains (see Section 1). The densest, fastest wind that can be accelerated by this mechanism is

$$\frac{L}{c} \gtrsim \dot{M}v, \qquad (1)$$

where the luminosity $L = 1585$ L$_\odot$ for EU Del (McDonald et al. 2012). For a 9.5 km s^{-1} wind, $\dot{M} \leq 3.4 \times 10^{-6}$ M$_\odot$ yr^{-1}. However, this limit does not take the stellar gravity into account. Escape velocity at the canonical dust-formation radius (≈ 2 R_*) is $\sim$21 km s^{-1}, which reduces the maximum mass-loss rate to $\dot{M} \lesssim 1.0 \times 10^{-6}$ M$_\odot$ yr^{-1}. The exact value depends on the actual dust-formation radius and the momentum already imparted to the escaping material by stellar pulsations.

In addition to these factors, only a fraction of the stellar light is reprocessed. McDonald et al. (2012) presented an SED compiled from literature photometry and spectroscopy for EU Del, showing the star to have a substantial infrared excess, with $\sim$1.4 per cent of light being reprocessed (McDonald et al. 2012). This reduces the upper limits such that $\dot{M} \lesssim 1.5 \times 10^{-8}$ M$_\odot$ yr^{-1} for a radiation-driven wind. The range of possible mass-loss rates is $\sim 10^{-8}$ to 10^{-7} (we remind the reader that formal errors are poorly determined). There is little overlap between the range of possible mass-loss rates from observations and the range that be sustained from radiation pressure on dust.

This $\sim$1.4 per cent can be increased if photons are scattered by large dust grains, rather than absorbed, as scattering does not change the overall shape of the SED (Höfner 2008). To better address radiation transport within the wind, we have modelled the SED of EU Del using the DUSTY radiative transfer code (Ivezic &

Elitzur 1997). DUSTY's `density-type = 3` setting computes a radiation-driven wind structure by solving the wind hydrodynamics, including dust drift, and computes limits where the gravitational attraction from the host star becomes important. We use a BT-SETTL model atmosphere at 3300 K, $\log(g) = 0$, [Fe/H] $= -0.5$ (Allard et al. 2003) to represent the underlying star (Fig. 1).

A radiative transfer dust model requires knowledge of the dust species involved. The infrared spectrum of EU Del shows very weak dust features. A weak feature may exist near 13 μm due to alumina (Sloan et al. 2003) and a 20-μm silicate feature is suggested by the rising spectrum between 15 and 20 μm, but it is difficult to determine whether these are real. Weak or absent features are typical of metal-poor stars in globular clusters (McDonald et al. 2009; Sloan et al. 2010; McDonald et al. 2011a,b). In globular clusters, metallic iron has been suggested to be the dominant component of such stars (McDonald et al. 2010), but carbonaceous grains remain an alternative possibility (Höfner & Andersen 2007). Since we cannot readily identify the dust species around EU Del, we explore several different options.

We have created four different DUSTY models. For all models, we assume a standard Mathis–Rumpl–Nordsiek size distribution (Mathis, Rumpl & Nordsieck 1977), i.e. that the number (n) of grains with size a is given by $n(a) \propto a^{-q}$ where q is typically 3.5. Typically, sizes are limited between 0.025 and 0.25 μm for silicate grains. DUSTY uses Mie theory to calculate the appropriate opacity. For all models, we assume that the dust:gas ratio is ∼1:372, based on scaling the solar-metallicity value of ∼1:200 to the [Fe/H] ∼ –0.27 metallicity derived above. Our modifications to this model are as follows.

(i) Pure metallic iron, using optical constants from Ordal et al. (1988), with grain size limits 0.005–0.03 μm (green, solid line in Fig. 1). A condensation temperature of 800 K is assumed. This reproduces the spectrum between 4 and 10 μm well, but fails to capture the excess emission between 10 and 25 μm. The small grain size is needed to reduce the 100-μm emission.

(ii) Pure amorphous carbon, using optical constants from Hanner (1988), with the same grain size (purple, dashed line in Fig. 1). A condensation temperature of 800 K is assumed. This fits the data between 3 and 4 μm better, but overestimates the 4–5 μm contribution and underestimates the 10–25 μm flux even more than the metallic iron model.

(iii) A mix of amorphous silicates (80 per cent; Draine & Lee 1984) and alumina (20 per cent; Begemann et al. 1997) with large grains. Grain sizes are limited to 0.005–1 μm, and a condensation temperature of 1000 K is assumed (grey, dotted line in Fig. 1). This underestimates the flux between 2 and 10 μm and at 25 μm and produces an unobserved 10-μm peak.

(iv) The same mix, but with a single population of 3-μm grains (black, dotted line in Fig. 1). This underestimates the flux between 2 and 10 μm, but reproduces the SED at all longer wavelengths.

The mixture of silicates to alumina in the final two models were varied, with the above 80:20 mixture best fitting the observed IR spectrum. A higher alumina ratio produces an unobserved 11-μm peak in preference to a 10-μm peak.

The fourth model is conceptually difficult to form, as it requires large silicate grains without any smaller silicate grains to form them from. We consider this model unlikely, but it may be physically possible if small alumina grains are coated with silicates. It seems likely that iron (or a similar species) contributes to the spectrum, in order to reproduce the 2–10 μm dust emission. Iron cannot condense near the star due to its high opacity (Bladh & Höfner 2012). A gradient of increasing iron content in silicate grains at larger radii from the star may be possible (Bladh et al. 2015). This would hold the grain temperature near the condensation temperature (∼1000 K), leading to a greater 2–10 μm emissivity than we model here. Some combination of all of these factors may lead to layered grains more complex than the grain population we model here.

The mass-loss rates derived from our fits are $\dot{M} = 5.7$, 1.3, 1.3 and $1.0 \times 10^{-7}\,\mathrm{M_\odot\,yr^{-1}}$, respectively. The latter three are similar to the CO mass-loss rate of $\sim 10^{-8}$ to $10^{-7}\,\mathrm{M_\odot\,yr^{-1}}$. Metallic iron produces a mass-loss rate greater than that measured (Section 2.4); however, we argue in the previous paragraph why this does not necessarily mean it is invalid.

Crucially, however, the expansion velocities in all cases are very small: only 2.1, 2.4, 7.5 and 5.5 $\mathrm{km\,s^{-1}}$, respectively. The metallic iron and amorphous carbon velocities are below the velocities at which the DUSTY models can be considered valid (5 $\mathrm{km\,s^{-1}}$) and far below the expansion velocity of the wind of EU Del (9.5 $\mathrm{km\,s^{-1}}$). Any increase in the wind velocity would require increasing the mass-loss rate proportionally and altering the velocity structure. The third (large-grained silicate–alumina conglomerate) model could achieve a 9.5 $\mathrm{km\,s^{-1}}$ wind velocity if the star were of solar metallicity; however, it fails to reproduce the observed spectrum. The fourth (3-μm silicate) model reaches 7.5 $\mathrm{km\,s^{-1}}$ at solar metallicity but, as noted, is physically difficult to create. More importantly, DUSTY does not account for the decrease in effectiveness due to stellar gravity. The minimum applicable mass ('$<M$') warning in the DUSTY software indicates that gravity has a substantial unmodelled effect on these models. We have explored a number of other options to try to reproduce the mass-loss rate and wind velocity observed without success.

We therefore conclude that EU Del is unlikely to have a primarily radiation-driven wind, although the velocity may be enhanced by radiation pressure on dust. Should a different energy source provide most of the power for the wind, the dust particles will not start from a resting levitated layer above the star. They will therefore spend less time in the radiation-driving zone. Hence, the time-integrated acceleration the wind experiences due to radiation pressure will be less than suggested by the velocities quoted above.

3.2 A magnetically driven wind

Without direct observation of the magnetic field strength and the stellar rotation period, it is difficult to reasonably determine the energy in a magnetically driven wind. Magnetic fields of luminous ($\sim 10^3\,\mathrm{L_\odot}$) giants tend to be weak (<1 G; Aurière et al. 2015), although a few individual stars have a field of a few Gauss (e.g. Lèbre et al. 2014; Sabin, Wade & Lèbre 2015). Rotation periods are sufficiently slow that the lines are not observably broadened.

An alternative approach is to compare to scaling relations based on empirical mass-loss rates. Relations such as those of Reimers (1975) and Schröder & Cuntz (2005) accurately represent mass-loss rates of stars across a large part of the Hertzsprung–Russell diagram where magnetic activity is thought to drive the stellar wind. These relations prescribe mass-loss rates (in $\mathrm{M_\odot\,yr^{-1}}$) of:

$$\dot{M}_{\mathrm{Reimers}} = 4 \times 10^{-13} \eta_{\mathrm{Reimers}} \frac{LR}{M} \tag{2}$$

and

$$\dot{M}_{\mathrm{SC}} = 4 \times 10^{-13} \eta_{\mathrm{SC}} \frac{LR}{M} \left(\frac{T_{\mathrm{eff}}}{4000\,\mathrm{K}} \right)^{3.5} \left(1 + \frac{g_\odot}{4300 g} \right), \tag{3}$$

where η_{Reimers} and η_{SC} are fitting parameters.

The value of η may depend on the environment under investigation and is likely a function of more parameters (e.g. Schröder & Cuntz 2005). In globular clusters, it is well calibrated on the red giant branch (RGB), at $\eta_{\rm Reimers} = 0.477 \pm 0.132$ and $\eta_{\rm SC} = 0.172 \pm 0.047$ (McDonald & Zijlstra 2015, including systematic errors). *Kepler* measurement of stars in the open cluster NGC 6791 suggests $0.1 \lesssim \eta_{\rm Reimers} \lesssim 0.3$ (Miglio et al. 2012).[5] L and R take the values from Table 1, which yields $\log(g) = 0.00$.

Adopting these values gives $\dot{M}_{\rm Reimers} = 6 \times 10^{-8}\,{\rm M}_\odot\,{\rm yr}^{-1}$ and $\dot{M}_{\rm SC} = 8 \times 10^{-8}\,{\rm M}_\odot\,{\rm yr}^{-1}$. These are within the range of mass-loss rates obtained from the CO lines, implying that magnetic energy could drive the wind. Whether it does so depends on whether these empirical laws accurately describe the transfer of magnetic energy to the wind of bright giant stars, which is uncertain.

Qualitatively, no indicators of a magnetically driven wind are present in the spectrum. Conventionally, magnetic heating of plasma above the surface produces a chromosphere (but not a full corona; Hartmann & MacGregor 1980). This chromosphere has a low filling factor, but exhibits emission components to chromospherically active lines (e.g. Dupree et al. 1994; McDonald & van Loon 2007; Mészáros, Avrett & Dupree 2009b). Such lines include Hα, Hβ, Hγ (etc.), the infrared calcium triplet, the Mg II K and Na II D lines. Emission components to these lines are variable in strength, but rarely disappear completely. No emission components are found in the optical spectrum of Valdes et al. (2004).

Emission components are normally observed to disappear in more luminous stars, probably when the chromosphere becomes destabilized by the stellar pulsation. They later give way to stronger, less structured emission lines as atmospheric shocks from the pulsations again heat the circumstellar environment (Dupree et al. 1984; McDonald & van Loon 2007). In conclusion, we cannot rule out a magnetically driven wind, but neither does it appear likely from qualitative indicators.

3.3 A pulsation-driven wind?

Over the course of the pulsation cycle, a fraction of the radiation from the stellar interior is trapped during the rising phase of the stellar pulsation and released during the falling phase. In a pulsation-driven wind, the kinetic energy given to the wind must be less than half the energy trapped by the stellar atmosphere during the pulsation cycle. Hence pulsations have sufficient energy to drive a wind if:

$$\frac{\dot{M}v^2}{L} < \frac{1}{2}\Delta, \tag{4}$$

where Δ is the peak-to-peak pulsation amplitude, measured as a fraction of the star's bolometric flux (van Loon 2002; van Loon et al. 2008a). This should be very similar to the light-curve amplitude at the peak of the star's SED. Light curves from the Diffuse Infrared Background Experiment (DIRBE), although of poor signal to noise (Price et al. 2010), show the amplitude of EU Del rises from ∼0.05 mag at 4.9 μm to ∼0.1 mag at 2.2 μm (see also Tabur et al. 2009). The amplitude increases further to ∼0.45 mag in the *Hipparcos* data at 0.53 μm (van Leeuwen 2007). The star's SED peak is in the *H* band. The *H*-band photometric amplitude is likely to be slightly larger than that at 2.2 μm, but smaller than the optical variation. Assuming the phase lag between the optical and infrared light curves is small, we can conservatively expect that the bolometric variability (Δ), is ∼10 per cent of the total intensity.

Half of this is available to drive the wind, or 1.2×10^{29} W. Were this energy liberated into the wind, it could support a mass-loss rate of a staggering $0.021\,{\rm M}_\odot\,{\rm yr}^{-1}$. As highlighted by van Loon et al. (2008a), only a tiny fraction (one part in $\sim 10^6$) of this needs to be liberated to drive the wind.

A more realistic estimate may come from pulsation growth rates. The dimensionless growth rate ($\dot{A}$) defines the fractional increase in pulsation amplitude per pulsation cycle. Since most stars have stable pulsation amplitudes, this defines the maximum fraction of pulsation energy that could be expended to drive material from the star (the remainder of which will likely heat the outer atmosphere), thus:

$$\frac{\dot{M}v^2}{L} < \frac{1}{2}\dot{A}\Delta. \tag{5}$$

For EU Del, we can expect growth rates of ∼10 per cent (Fox & Wood 1982; Ya'Ari & Tuchman 1996; Xiong & Deng 2007), meaning $\sim 10^{28}$ W is available to drive the wind: substantially more than the $\gtrsim 5.6 \times 10^{23}$ W mentioned at the start of Section 3.

Of the energy expended by the stellar pulsation, almost all of it is required to overcome the gravitation potential of the star. The pulsation-enhanced, dust-driven wind model already relies on pulsation to provide half of this energy to levitate material from the stellar surface to $\sim 2\,{\rm R}_*$, so it is not unreasonable to suppose it can provide the remaining half as well. Radiation pressure would then become a small additional component, creating a pulsation-P*driven*, dust-*enhanced* wind.

Expansion velocity profiles of luminous evolved stars are not consistent with this pulsation-driven scenario (e.g. Richards et al. 2012). However, these stars have greater mass-loss rates ($\sim 10^{-5}\,{\rm M}_\odot\,{\rm yr}^{-1}$) and faster wind velocities ($\sim$10–30 km s^{-1}) than we observe here. They are typically either massive supergiants with weaker, stochastic pulsations, or heavily obscured AGB stars where trapped radiation can be more effective in driving a wind. While radiation pressure on winds may therefore be effective in these environments, they may not be effective in strongly pulsating but less obscured stars like EU Del. Given the difficulty of the other methods to drive a wind from EU Del, we suggest the dominant driving mechanism for the wind of this low-luminosity AGB star is the pulsation itself.

4 DISCUSSION

4.1 Comparison to VY Leo

Few other giant stars of similar luminosity have been observed in these CO transitions. The closest literature comparison to EU Del is VY Leo (HIP 53449). Table 3 compares the properties of the two stars, and Fig. 3 shows their SEDs. VY Leo is probably a little less evolved, having a slightly higher temperature and lower luminosity, giving it a slightly smaller radius. The photometry for these SEDs is derived from: *Hipparcos* (Perryman & ESA 1997; van Leeuwen 2007), the *Cosmic Background Explorer/Diffuse Infrared Background Experiment* (COBE/DIRBE; Price et al. 2010), the American Association of Variable Star Observers All-Sky Photometric Survey (APASS; Henden et al. 2012), Johnson et al. (1966), Morel & Magnenat (1978), Warren (1991), the Two Micron All Sky Survey (2MASS; Skrutskie et al. 2006), *Akari* (Ishihara et al. 2010), the *Wide-field Infrared Survey Explorer* (*WISE*; Cutri et al. 2012), the *Infrared Astronomical Satellite* (*IRAS*; Neugebauer et al. 1984)

[5] However, it is likely that $\eta_{\rm Reimers} \sim 0.1$ would be sufficiently low to delay most mass-loss to the dust-enshrouded 'superwind' phase of the AGB. This enhanced 'superwind' is not seen in NGC 6791 (van Loon, Boyer & McDonald 2008b).

Table 3. Stellar parameters of EU Del compared to VY Leo

Parameter	EU Del	VY Leo	Ref.
Distance (d)	117 ± 7 pc	119 ± 5 pc	1
Tangential velocity	38 km s^{-1}	14 km s^{-1}	1
Radial velocity	-66 km s^{-1}	-8.39 km s^{-1}	2
Spectral type	M6	M5.5	2
Effective temperature ($T_{\rm eff}$)	3243 K	3300 K	3
	3227 K	3311 K	4
		3300 K	5
Luminosity (L)	1585 $L_\odot$	1357 $L_\odot$	4
		1346 $L_\odot$	5
log(g)	0.39	1.00	6,3
		0.20	7
Radius (R)	127.5 $R_\odot$	112.1 $R_\odot$	4
Escape velocity ($M = 0.6\,M_\odot$)	42 km s^{-1}	45 km s^{-1}	
$W_{\rm JK}$ at LMC	11.20 mag	11.56 mag	[a]
Variability type	SRV (O-rich)	Irregular/SR	8,9
Pulsation period	60.8, 132.6, 235.3, 67.3, 44.0 d	54.9, 84.5, 75.0, 35.8 d	10
Amplitude (optical)	149, 113, 91, 75, 61 mmag	162, 76, 69, 69 mmag	10
Pulsation mode	C′, C, ?, C′, D/E?	C′, F?, F?, B?	
Derived mass	1.80, *0.76*, 0.40, 1.61, 2.59 $M_\odot$	1.53, *0.95*, 1.08, 2.46 $M_\odot$	11[b]
Outflow velocity	9.505 ± 0.021 km s^{-1}	12.00 ± 0.35 km s^{-1}	11,12
CO (2–1) flux	76.3 ± 1.5 Jy km s^{-1}	8.1 ± 0.5 Jy km s^{-1}	11,12
CO (3–2) flux	146.5 ± 3.3 Jy km s^{-1}	4.9 ± 0.8 Jy km s^{-1}	11,12
Mass-loss rate	few $\times\ 10^{-8}$ $M_\odot$ yr^{-1}	few $\times\ 10^{-9}$ $M_\odot$ yr^{-1}	11,12

References: (1) van Leeuwen (2007); (2) Anderson & Francis (2012); (3) Cesetti et al. (2013); (4) McDonald et al. (2012); (5) Groenewegen (2012); (6) Wu et al. (2011); (7) Ivanov et al. (2004); (8) Mennessier et al. (2001); (9) Watson (2006); (10) Tabur et al. (2009); (11) this work; (12) Groenewegen (2014). [a]$W_{\rm JK}$ is a reddening-free Wesenheit index in the 2MASS J and $K_{\rm s}$ bands. Here, it is given *at the distance of the Large Magellanic Cloud* (LMC; 50 kpc) for easy comparison to Wood (2015). [b]Derived masses are based on the period–mass–radius relationship of Wood (1990) for the different periods found by Tabur et al. (2009). Italic type indicates the adopted mass based on our assignment of the fundamental-mode period.

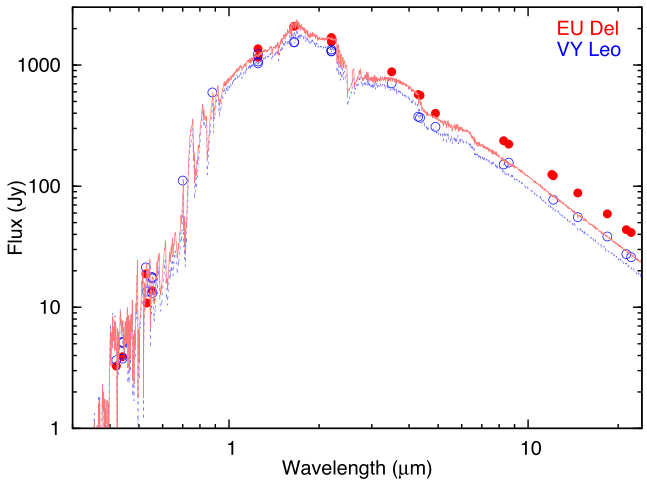

Figure 3. SED of EU Del and VY Leo (large red and blue points, respectively). EU Del is shown with a BT-SETTL model atmosphere at 3300 K, log(g) = 0.5 dex, [Fe/H] = −0.5 dex (red line). The model for VY Leo is at 3200 K, log(g) = 1.0 dex, [Fe/H] = 0 dex (dashed blue line). See text for the sources of the data.

and the *Midcourse Space Experiment* (*MSX*; Egan & Price 1996). As with EU Del, reddening to VY Leo has been neglected. Based on the extinction maps of Lallement et al. (2014), $E(B-V)$ is likely to be <0.01.

Spectroscopically, VY Leo is very similar to EU Del, although VY Leo shows a much more modest infrared excess (Groenewegen 2012). This is commensurate with the lower mass-loss rate derived from its fainter CO lines. VY Leo pulsates with a slightly shorter period. Notably, VY Leo does not have significant power in longer period modes, while EU Del does. Power in shorter period pulsation modes is typically associated with stars of a higher mass (e.g. Wood 2015).

The log(g) estimates disagree to the extent that it is impossible to define which is the more massive star. However, stellar mass can be estimated from the pulsation period via the period–mass–radius relationship of Wood (1990):

$$\log P = -2.07 + 1.94 \log R - 0.9 \log M, \qquad (6)$$

where period is in days, and radius and mass are in solar units. This calculation refers to the fundamental mode period. Table 3 lists the resulting masses if each pulsation mode was adopted as the fundamental mode. The italic type (0.76 $M_\odot$ for EU Del and 0.95 $M_\odot$ for VY Leo) indicates the mass corresponding to our identification of the fundamental mode for each star.

Table 3 also lists our identification of the pulsation modes for EU Del and VY Leo, based on the positions of these modes in the period–luminosity diagram of Wood (2015). We use labels for the period–luminosity sequences from Wood (2015), where sequence C is generally accepted as the fundamental mode, and C′, B and A are overtone modes. The origins of sequence F are not clear, but Wood (2015) suggests this is the higher mass counterpart of the fundamental mode.

EU Del appears to be an overtone (sequence C′) pulsator, with the fundamental period being 132.6 d. The fundamental and overtone modes are shifted to the shorter period side of sequences B and C, as is normal for an overtone pulsator (see Wood 2015, his fig. 4).

VY Leo is harder to place. The fundamental mode is not clear, as no mode in sequence C seems to be excited. Two modes bracketing

sequence B are excited, as are two modes within the sequence F region. If sequence F represents the fundamental mode, a mass of ∼0.95 or 1.08 $M_\odot$ is implied for VY Leo. We have highlighted the mass corresponding to the slightly stronger 84.5-day period (0.95 $M_\odot$) in Table 3. This would make VY Leo a more massive star.

For stars of the same luminosity, an observational correlation exists between power in longer period, fundamental modes and the red infrared colours which indicate strong stellar mass-loss (Boyer et al. 2015, their fig. 17). At the same luminosity, more massive stars have shorter period pulsations. This is true of both their fundamental pulsation period (equation 6, Wood 1990) and mode in which they pulsate (Fox & Wood 1982, their table 2). Therefore, at a given luminosity, longer pulsation periods imply lower stellar masses and higher mass-loss rates. Hence, strong mass-loss will start earlier in lower mass stars, driven by their long-period pulsations. Also, at any particular luminosity, a low-mass star will have stronger mass-loss than its high-mass equivalent.

In comparing EU Del and VY Leo, the increase in mass-loss rate appears to be caused by the more effective long-period pulsations driving mass-loss. Hence, this provides additional evidence that the wind of EU Del is driven by pulsations. Pulsation likely does not enhance the wind of VY Leo, hence it has a lower mass-loss rate. While EU Del does not appear to be supported by a magnetically driven wind (Section 3.2), VY Leo may be. Whatever the driving mechanisms involved, the similarity between the outflow velocities of EU Del and VY Leo adds support to our claim that radiation pressure on dust is ineffective.

4.2 Testable predictions for stellar mass-loss

We can now turn to other samples to examine the hypothesis of a pulsation-driven dust-enhanced wind. Pulsation amplitude and period are strong functions of effective temperature [Kjeldsen & Bedding 1995 and equation (6), respectively]. Effective temperature is a function of atmospheric opacity and hence metallicity. Thus, if pulsation amplitude and period are linked to mass-loss rate, we would expect pulsation-driven winds to depend strongly on metallicity. However, the mass-loss rates of metal-poor RGB stars at these luminosities are largely metallicity independent (McDonald & Zijlstra 2015). This independence implies that pulsation-driven winds are not important on the RGB, and that the transition to a dust-producing, pulsation-driven wind only happens on the AGB. This would be observable in the luminosity distribution of dusty sources across the RGB tip. While the luminosity function of all stars decreases as one moves to brighter stars above the RGB tip, the luminosity function of AGB stars should not. This is tentatively observed in globular clusters already (e.g. McDonald et al. 2011a; Momany et al. 2012).

Stellar wind theory dictates that, in a pulsation-enhanced, dust-driven wind, the mass-loss rate is set by the pulsations, but the terminal velocity is set by the radiation pressure on dust (e.g. Lamers & Cassinelli 1999; Nugis & Lamers 2002). Numerous observations show that more luminous, dustier stars have faster winds, but that few single stars have CO lines with velocities below ∼5–10 km s^{-1} (e.g. Young 1995; Knapp et al. 1998).

Few direct observations of terminal wind velocities exist in single stars without pulsation-enhanced winds, due to their low mass-loss rates and lack of condensed molecules. There are indirect measurements from asymmetries in chromospherically active lines (McDonald & van Loon 2007; Mészáros, Dupree & Szentgyörgyi 2008; Mészáros, Dupree & Szalai 2009a). The absorption cores of these lines form above the stellar chromosphere, but typically before the winds have reached their terminal velocity. They typically show a velocity of a few km s^{-1} just above the stellar surface, again increasing with luminosity. Near-IR He I line observations of early AGB stars indicate a much faster terminal velocity (∼30–100 km s^{-1}; Dupree, Smith & Strader 2009), implying that the terminal velocity should *decrease* with increasing luminosity in the early-AGB phase, but these are difficult measurements that are hard to confirm.

We can therefore expect that terminal wind velocities of early-AGB stars are either stable and low, or decline with luminosity. There should then exist an inflection point, or a velocity minimum, after which the wind velocities increase in response to dust driving. This point should be reached at higher luminosities in metal-poor stars. EU Del and VY Leo should straddle this inflection, which probably occurs near 10 km s^{-1}. Further measurements of early-M-type stars likely to occupy this transition region would determine when dust driving is likely to begin. Identification of this point will require accurate luminosities for these sources, which will require accurate distances.

5 CONCLUSIONS

We have observed the CO outflow from EU Del, finding a wind close to the canonical 10 km s^{-1} but with a mass-loss rate of a few $\times 10^{-8}$ $M_\odot$ yr^{-1}. The metallicity and kinematic origin of EU Del require further refinement. We project it to a relatively metal-poor member of the thin disc population of our Galaxy, although the uncertainty on the metallicity is significant. Using physical arguments, and by comparison to the similar star VY Leo, we suggest that the wind of EU Del is largely driven by stellar pulsation. Radiation pressure on dust does not appear to modify the outflow velocity. We suggest that EU Del is a low-mass AGB star that has recently started strong enough mass-loss to initiate dust production, thanks to excitation of its 132.6-day, fundamental-mode pulsation. We encourage further observations of CO and dust production around stars near the RGB tip to identify the link between pulsation, stellar mass and mass-loss rate.

ACKNOWLEDGEMENTS

This publication is based on data acquired with the Atacama Pathfinder Experiment (APEX). APEX is a collaboration between the Max-Planck-Institut fur Radioastronomie, the European Southern Observatory and the Onsala Space Observatory. Based on observations made with ESO telescopes under programme IDs 092.F-9328 and 094.F-9328. CIJ gratefully acknowledges support from the Clay Fellowship, administered by the Smithsonian Astrophysical Observatory. The authors are extremely grateful to Sofia Ramstedt, who reduced the data for this project, both for her work on the data and for her insightful comments during the preparation of this manuscript.

REFERENCES

Allard F., Guillot T., Ludwig H.-G., Hauschildt P. H., Schweitzer A., Alexander D. R., Ferguson J. W., 2003, in Martín E., ed., Proc. IAU Symp. 211, Brown Dwarfs. Astron. Soc. Pac., San Francisco, p. 325
Anderson E., Francis C., 2012, Astron. Lett., 38, 331
Aurière M. et al., 2015, A&A, 574, A90
Begemann B., Dorschner J., Henning T., Mutschke H., Guertler J., Koempe C., Nass R., 1997, ApJ, 476, 199

Bladh S., Höfner S., 2012, A&A, 546, A76
Bladh S., Höfner S., Aringer B., Eriksson K., 2015, A&A, 575, A105
Boyer M. L., McDonald I., Srinivasan S., Zijlstra A., van Loon J. T., Olsen K. A. G., Sonneborn G., 2015, ApJ, 810, 116
Cesetti M., Pizzella A., Ivanov V. D., Morelli L., Corsini E. M., Dalla Bontà E., 2013, A&A, 549, A129
Cutri R. M. et al., 2012, Technical report, Explanatory Supplement to the WISE All-Sky Data Release Products. The Infrared Processing and Analysis Center (IPAC), Caltech
de Bruijne J. H. J., Eilers A.-C., 2012, A&A, 546, A61
Draine B. T., Lee H. M., 1984, ApJ, 285, 89
Dupree A. K., Hartmann L., Avrett E. H., 1984, ApJ, 281, L37
Dupree A. K., Hartmann L., Smith G. H., Rodgers A. W., Roberts W. H., Zucker D. B., 1994, ApJ, 421, 542
Dupree A. K., Smith G. H., Strader J., 2009, AJ, 138, 1485
Edvardsson B., Andersen J., Gustafsson B., Lambert D. L., Nissen P. E., Tomkin J., 1993, A&A, 275, 101
Egan M. P., Price S. D., 1996, AJ, 112, 2862
Fox M. W., Wood P. R., 1982, ApJ, 259, 198
Frogel J. A., Stephens A., Ramírez S., DePoy D. L., 2001, AJ, 122, 1896
Gilmore G., Reid N., 1983, MNRAS, 202, 1025
Girardi L. et al., 2010, ApJ, 724, 1030
Gratton R. G., Sneden C., Carretta E., Bragaglia A., 2000, A&A, 354, 169
Groenewegen M. A. T., 2012, A&A, 540, A32
Groenewegen M. A. T., 2014, A&A, 561, L11
Habing H. J., 1996, A&AR, 7, 97
Hanner M., 1988, Technical Report, Grain Optical Properties. Jet Propulsion Laboratory (JPL), Pasadena
Hartmann L., MacGregor K. B., 1980, ApJ, 242, 260
Henden A. A., Levine S. E., Terrell D., Smith T. C., Welch D., 2012, J. Am. Assoc. Var. Star Obs., 40, 430
Höfner S., 2008, A&A, 491, L1
Höfner S., Andersen A. C., 2007, A&A, 465, L39
Ishihara D. et al., 2010, A&A, 514, A1
Ivanov V. D., Rieke M. J., Engelbracht C. W., Alonso-Herrero A., Rieke G. H., Luhman K. L., 2004, ApJS, 151, 387
Ivezić Ž., Beers T. C., Jurić M., 2012, ARA&A, 50, 251
Ivezic Z., Elitzur M., 1997, MNRAS, 287, 799
Johnson H. L., Mitchell R. I., Iriarte B., Wisniewski W. Z., 1966, Commun. Lunar Planet. Lab., 4, 99
Keenan P. C., McNeil R. C., 1989, ApJS, 71, 245
Kjeldsen H., Bedding T. R., 1995, A&A, 293, 87
Knapp G. R., Young K., Lee E., Jorissen A., 1998, ApJS, 117, 209
Lallement R., Vergely J.-L., Valette B., Puspitarini L., Eyer L., Casagrande L., 2014, A&A, 561, A91
Lamers H. J. G. L. M., Cassinelli J. P., 1999, Introduction to Stellar Winds. Cambridge Univ. Press, Cambridge
Lèbre A., Aurière M., Fabas N., Gillet D., Herpin F., Konstantinova-Antova R., Petit P., 2014, A&A, 561, A85
McDonald I., van Loon J. T., 2007, A&A, 476, 1261
McDonald I., Zijlstra A. A., 2015, MNRAS, 448, 502
McDonald I., van Loon J. T., Decin L., Boyer M. L., Dupree A. K., Evans A., Gehrz R. D., Woodward C. E., 2009, MNRAS, 394, 831
McDonald I., Sloan G. C., Zijlstra A. A., Matsunaga N., Matsuura M., Kraemer K. E., Bernard-Salas J., Markwick A. J., 2010, ApJ, 717, L92
McDonald I. et al., 2011a, ApJS, 193, 23
McDonald I. et al., 2011b, MNRAS, 417, 20
McDonald I., Boyer M. L., van Loon J. T., Zijlstra A. A., 2011c, ApJ, 730, 71
McDonald I., Zijlstra A. A., Boyer M. L., 2012, MNRAS, 427, 343
Mamon G. A., Glassgold A. E., Huggins P. J., 1988, ApJ, 328, 797
Marigo P., Girardi L., Bressan A., Groenewegen M. A. T., Silva L., Granato G. L., 2008, A&A, 482, 883
Markwardt C. B., 2009, in Bohlender D. A., Durand D., Dowler P., eds, ASP Conf. Ser. Vol. 411, Astronomical Data Analysis Software and Systems XVIII. Astron. Soc. Pac., San Francisco, p. 251
Mathis J. S., Rumpl W., Nordsieck K. H., 1977, ApJ, 217, 425
Mennessier M. O., Mowlavi N., Alvarez R., Luri X., 2001, A&A, 374, 968
Mészáros S., Dupree A. K., Szentgyörgyi A., 2008, AJ, 135, 1117
Mészáros S., Dupree A. K., Szalai T., 2009a, AJ, 137, 4282
Mészáros S., Avrett E. H., Dupree A. K., 2009b, AJ, 138, 615
Meyer M. R., Edwards S., Hinkle K. H., Strom S. E., 1998, ApJ, 508, 397
Miglio A. et al., 2012, MNRAS, 419, 2077
Momany Y., Saviane I., Smette A., Bayo A., Girardi L., Marconi G., Milone A. P., Bressan A., 2012, A&A, 537, A2
Morel M., Magnenat P., 1978, A&AS, 34, 477
Neugebauer G. et al., 1984, ApJ, 278, L1
Nugis T., Lamers H. J. G. L. M., 2002, A&A, 389, 162
Ordal M. A., Bell R. J., Alexander R. W., Jr, Newquist L. A., Querry M. R., 1988, Appl. Opt., 27, 1203
Perryman M. A. C. et al., 1997, A&A, 323, L49
Price S. D., Smith B. J., Kuchar T. A., Mizuno D. R., Kraemer K. E., 2010, ApJS, 190, 203
Ramírez S. V., Stephens A. W., Frogel J. A., DePoy D. L., 2000, AJ, 120, 833
Ramstedt S., Olofsson H., 2014, A&A, 566, A145
Ramstedt S., Schöier F. L., Olofsson H., Lundgren A. A., 2008, A&A, 487, 645
Reddy B. E., Lambert D. L., 2005, AJ, 129, 2831
Reimers D., 1975, Mem. Soc. R. Sci. Liege, 8, 369
Richards A. M. S., Etoka S., Gray M. D., Lekht E. E., Mendoza-Torres J. E., Murakawa K., Rudnitskij G., Yates J. A., 2012, A&A, 546, A16
Roediger J. C., Courteau S., Graves G., Schiavon R., 2014, ApJS, 210, 10
Sabin L., Wade G. A., Lèbre A., 2015, MNRAS, 446, 1988
Samus N. N., Durlevich O. V., Zharova A. V., Kazarovets E. V., Kireeva N. N., Pastukhova E. N., Williams D. B., Hazen M. L., 2006, Astron. Lett., 32, 263
Schröder K.-P., Cuntz M., 2005, ApJ, 630, L73
Skrutskie M. F. et al., 2006, AJ, 131, 1163
Sloan G. C., Price S. D., 1995, ApJ, 451, 758
Sloan G. C., Kraemer K. E., Goebel J. H., Price S. D., 2003, ApJ, 594, 483
Sloan G. C. et al., 2010, ApJ, 719, 1274
Soubiran C., Le Campion J., Cayrel de Strobel G., Caillo A., 2010, A&A, 515, A111
Tabur V., Bedding T. R., Kiss L. L., Moon T. T., Szeidl B., Kjeldsen H., 2009, MNRAS, 400, 1945
Valdes F., Gupta R., Rose J. A., Singh H. P., Bell D. J., 2004, ApJS, 152, 251
van Leeuwen F., 2007, A&A, 474, 653
van Loon J. T., 2002, in van Leeuwen F., Hughes J. D., Piotto G., eds, ASP Conf. Ser. Vol. 265, Omega Centauri, A Unique Window into Astrophysics. Astron. Soc. Pac., San Francisco, p. 129
van Loon J. T., Cohen M., Oliveira J. M., Matsuura M., McDonald I., Sloan G. C., Wood P. R., Zijlstra A. A., 2008a, A&A, 487, 1055
van Loon J. T., Boyer M. L., McDonald I., 2008b, ApJ, 680, L49
Vlemmings W. H. T. et al., 2013, A&A, 556, L1
Wallace L., Hinkle K., 1997, ApJS, 111, 445
Wallace L., Meyer M. R., Hinkle K., Edwards S., 2000, ApJ, 535, 325
Warren W. H., Jr 1991, Photoelectric Photometric Catalogue of Homogeneous Means in the UBV System (Mermilliod 1991). NASA, Greenbelt, MD
Watson C. L., 2006, Soc. Astron. Sci. Annu. Symp., 25, 47
Winters J. M., le Bertre T., Jeong K. S., Helling C., Sedlmayr E., 2000, A&A, 361, 641
Woitke P., 2006, A&A, 460, L9
Wood P. R., 1990, in Mennessier M. O., Omont A., eds, From Miras to Planetary Nebulae: Which Path for Stellar Evolution? Editions Frontieres, Gif-sur-Yvette, France, p. 67
Wood P. R., 2015, MNRAS, 448, 3829
Wu Y., Singh H. P., Prugniel P., Gupta R., Koleva M., 2011, A&A, 525, A71
Xiong D. R., Deng L., 2007, MNRAS, 378, 1270
Ya'Ari A., Tuchman Y., 1996, ApJ, 456, 350
Young K., 1995, ApJ, 445, 872

This paper has been typeset from a TEX/LATEX file prepared by the author.